Hole Mobility Enhancement Mechanism of Wurtzite GaN/AlN Heterojunction Quantum Well Under Tensile and Compressive Stresses

Xiyue Li, Yaqun Liu, Jing Wang, Everett Wang, *Member, IEEE*, and Gary Zhang, *Member, IEEE*

***Abstract*— The hole mobility enhancement mechanism of wurtzite (0001)-oriented gallium nitride (GaN)/AlN heterojunction quantum well (QW) under stress engineering is investigated to overcome the low hole mobility, which is considered to be the fundamental obstacle toward the realization of GaN-based complementary electronics. The hole mobility model is obtained by the six-band stress-dependent $k \times p$ Hamiltonian and the Kubo–Greenwood formula, taking the scattering rates of acoustic phonon, polar optical phonon, and surface roughness into account. Using these methods, the microscopic relationship between stress and hole mobility can be predicted according to the variation of 2-D valence subband dispersion. We demonstrate that the biaxial tensile stress is not a desirable way in the hole mobility enhancement because a large compressive strain induced by the pseudomorphic GaN/AlN heterointerface has to be overcome. We also find that due to the efficient achievements in both effective mass reduction and hole scattering suppression, the uniaxial compressive stress along the current channel and the uniaxial tensile stress perpendicular to the current channel can increase the hole mobility significantly. Under the combined effect of these two 8 GPa non-exclusive mechanisms, a sevenfold mobility enhancement can be obtained, up to the theoretical value of 190 cm^2/Vs at room temperature.**

***Index Terms*— Heterojunction quantum well (QW), hole mobility, scattering suppression, six-band $k \cdot \times p$ method, subband energy dispersion, wurtzite gallium nitride (GaN)/AlN.**

I. Introduction

GALLIUM nitride (GaN) has attracted considerable attention as a candidate material for both millimeter wave and high-power switching applications because of its large bandgap, high breakdown voltage, high electron mobility, and high thermal stability [1], [2], [3], [4], [5]. Despite GaN high electron mobility transistors (HEMTs) having been expected to be dominant in the next-generation power switching and radio frequency amplification, the widespread adoption of GaN for applications such as complementary and high-power conversion devices remains insufficient due to the imbalance between electron and hole mobility. Recently, many groups have demonstrated p-type GaN film and p-channel GaN-based field effect transistors using pulsed sputtering deposition (PSD) [6], [7], metal organic vapor phase epitaxy (MOVPE) [8], metal organic chemical vapor deposition (MOCVD) [9], [10], and molecular beam epitaxy (MBE) [11], [12]. The monolithic GaN-based complementary metal oxide semiconductor (CMOS) inverter circuits were also successfully demonstrated by Chu et al. [13], Nakajima et al. [14], and Zheng et al. [15]. However, the GaN exhibits comparatively low hole mobility usually below 40 cm^2/Vs at room temperature. In order to overcome these urgent technical demands, material engineering approaches aimed at increasing the hole mobility of GaN are needed.

The two key obstacles toward this goal are the large hole-effective mass of wurtzite GaN and various types of scattering. A common approach to improving the carrier mobility of semiconductors is via strain engineering. Poncé et al. [16], [17] found that the split-off (SO) band can be raised above the heavy hole (HH) and light hole (LH) band by applying biaxial tensile strain in (0001) plane, resulting in an obvious increase in hole mobility of bulk GaN. Gupta et al. [18] also showed that the uniaxial compressive strain is efficient in effective mass reduction and mobility enhancement. On the scattering side, Bader et al. [19] revealed that the available scattering density of states (DOS) can be reduced by the uniaxial tensile strain along the current flow. The six-band Hamilton [20] and EPW (Electron-Phonon coupling using Wannier functions) software [21] were also used to calculate the hole-phonon scattering rates of GaN. Analytical models have also been developed to describe the hole transport properties in a wide doping and temperature range accurately [22], [23].

Since the energy band diagram can be modified by stress engineering [24], [25], [26], it provides a practical and simple method to evaluate the variation of holes concentration and effective mass. Among the various structures proposed as a platform for p-channel nitride electronics,

Manuscript received 19 May 2023; revised 16 June 2023; accepted 21 June 2023. Date of publication 4 July 2023; date of current version 25 July 2023. This work was supported by the National Key Research and Development Program of China under Grant 2018YFB1802100. The review of this article was arranged by Editor G. M. Ghione. *(Xiyue Li and Yaqun Liu contributed equally to this work.) (Corresponding author: Xiyue Li.)*

Xiyue Li, Yaqun Liu, Jing Wang, and Gary Zhang are with the School of Integrated Circuits, Guangzhou Mega Center, Guangdong University of Technology, Guangzhou 510006, China (e-mail: lixiyue915@gdut.edu.cn).

Everett Wang is with the Beijing Institute of Nanoenergy and Nanosytems, Chinese Academy of Sciences, Beijing 101400, China.

Color versions of one or more figures in this article are available at https://doi.org/10.1109/TED.2023.3289791.

Digital Object Identifier 10.1109/TED.2023.3289791

the polarization-induced 2-D hole gas (2DHG) at GaN/AlN heterostructure has received recent attention because of the very high 2DHG density, the high thermal conductively, and the high breakdown electric field of GaN and AlN [27], [28]. In this work, the hole mobility enhancement mechanism of wurtzite GaN/AlN quantum well (QW) is described. We perform a comprehensive set of physical models to explain the hole mobility response under tensile and compressive stresses. The effect of various types of scattering, such as the acoustic phonon scattering, the polar optical phonon scattering, and the surface roughness scattering, is also considered. We construct a six-band stress-dependent quantum $k \times p$ method to elucidate the physics underlying the effect of stress on valence energy dispersion. The transport model based on Kubo–Greenwood formula is proposed to determine the behavior of hole mobility confined in a triangular well.

This article is organized as follows. We discuss how the tensile and compressive stresses alter the valence energy dispersion and hole effective mass in Section II. The temperature-dependence mobility behavior and the influence of stress on mobility gain are presented in Section III. Finally, we conclude our results in Section IV.

II. Bulk and Quantized Valence Subband Dispersion Under Stress

The quantized valence subband structure model of the wurtzite (0001)-oriented GaN/AlN heterojunction QW is performed using the six-band stress-dependent $k \times p$ Hamiltonian and the self-consistent Poisson–Schrödinger equations. The finite-difference method is utilized to discretize the Schrödinger equation on a mesh in the c-axis direction with N_z nodes, turning into an eigenvalue problem of a 6 $\times$6 N_z complex band Hermitian matrix to propose the 2-D iso-energy contours. The detailed description about the method is provided in our previous work [29], [30].

Following [27], the structure of the GaN/AlN heterojunction is described as a 13 nm GaN layer on top of a 400 nm AlN substrate. The thickness of the 2DHG is assumed to be 2 nm. The GaN epitaxial layer is fully, biaxially, and compressively strained (by 2.4%) to the underlying AlN layer. Such a case is regarded as "no external stress" in this article. This initial strain has not been considered in our previous work [30] and is therefore a critical improvement on the model.

Under the usual device operation, the carriers are spread in regions of low energy around the Γ point. Fig. 1 shows the 50 meV 3-D iso-energy surfaces of the bulk HH band under various types of stress. The transport plane, also the "in-plane," is set at the symmetry of the upper and lower halves, while the "off-plane" means other crystal orientations. Two kinds of stress are considered, including the biaxial stress and uniaxial stress. The polarization difference ($P_{sp}^{GaN} - P_{sp}^{AlN} + P_{pz}^{GaN}$) constitutes the 2DHG. The spontaneous and piezoelectric polarization constants are obtained in [31]. The energy patterns under non-stress, biaxial tensile stress, and biaxial compressive stress are completely isotropic. But the energies are moved down under biaxial compression and moved up under biaxial tension. Therefore, it can be estimated that the holes concentration repopulation from off-plane to in-plane is observed under

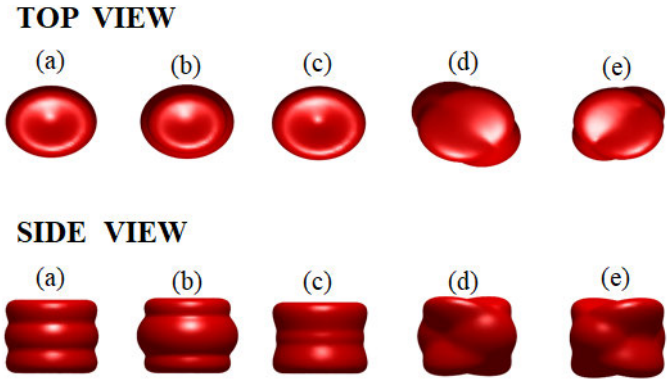

Fig. 1. Top and side views of bulk HH iso-energy surfaces at 0.5 eV under. (a) Non-stress. (b) Biaxial compressive stress. (c) Biaxial tensile stress. (d) Uniaxial compressive stress. (e) Uniaxial tensile stress.

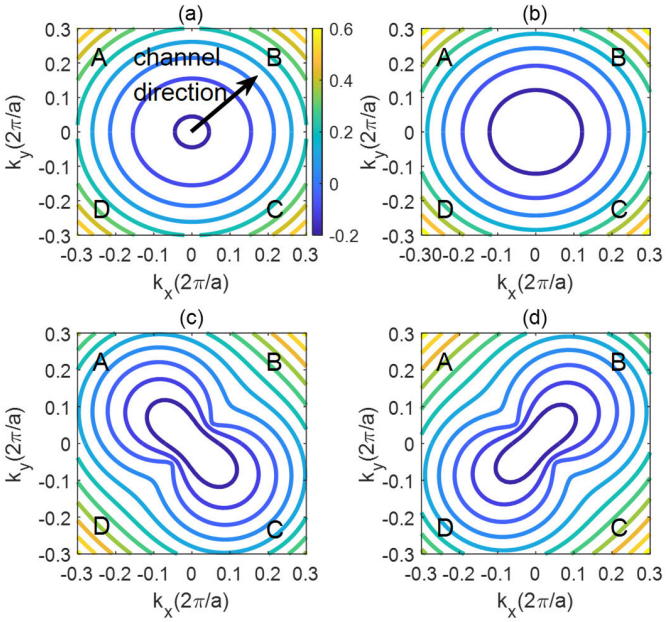

Fig. 2. Two-dimensional iso-energy contours of the first subband separated by 50 meV in (0001) transport plane under. (a) 8 GPa external biaxial tensile stress. (b) Biaxial compressive stress. (c) Uniaxial compressive stress. (d) Uniaxial tensile stress, respectively.

biaxial compressive stress, resulting in a stronger scattering process and the mobility degradation. In contrast, the biaxial tensile stress leads to the opposite conclusion. The holes are redistributed from in-plane to off-plane, thus reducing the scattering. However, since the hole mobility lies in a combination of the hole effective mass and the density of final states available for scattering, it is essential to extract the microscopic relationship between the stress and effective mass.

The 2-D iso-energy contours of the first subband under various types of stress can be seen in Fig. 2. The values of the stress are all set to 8 GPa. This is not a special value. It is only used to show the trend of energy distribution variation under stress. A thick arrow is used to indicate the current channel, since such direction is common in PMOS technology [32]. The slightly change in effective mass can be predicted because the shape of the first subband remains isotropic under both external biaxial tensile stress and biaxial compressive stress, as can be seen in Fig. 2(a) and (b). By extracting the second derivative of E-k dispersion along

TABLE I
HOLE EFFECTIVE MASS ALONG AND PERPENDICULAR TO THE CHANNEL DIRECTION (UNIT OF m_0)

External Stress Options	Along channel (B, D)	Perpendicular to channel (A, C)
8GPa Uniaxial Tensile Stress	2.181	0.328
8GPa Uniaxial Compressive Stress	0.194	0.357

TABLE II
VALUES OF STRAIN TENSORS UNDER VARIOUS TYPES OF EXTERNAL 8 GPA STRESS (THE "-" SIGN INDICATES THE COMPRESSIVE STRAIN)

	Uniaxial Compressive	Uniaxial Tensile	Biaxial Compressive	Biaxial Tensile
The biaxial component ε_{xx}	-3.66%	-1.15%	-4.07%	-0.73%
The biaxial component ε_{yy}	-3.66%	-1.15%	-4.07%	-0.73%
The shear component ε_{xy}	-1.90%	1.90%	0	0

the channel direction, the effective mass change from 1.845 m_0 (no external stress) to 1.858 m_0 (biaxial tension) and 1.842 m_0 (biaxial compression), respectively. Under these circumstances, the mobility gain contributed from effective mass is relatively weak. The mobility behavior then depends on the superposition of a minor effective mass contribution and the scattering contribution that is predominant.

Then, we examine the effect induced by in-plane uniaxial compressive and tensile stresses along the current channel. Since the shear stress, which is the difference between biaxial stress and uniaxial stress, can break crystal symmetry and induce carrier repopulation among different directions in the reciprocal space, the innermost contours near Γ point are ellipses rather than circles, as can be seen in Fig. 2(c) and (d). This is the signature of the fact that the energy distribution is not isotropic at all. The hole effective mass are shown in Table I. Under external uniaxial compressive stress, the hole effective mass along and perpendicular to the current direction are 0.194 and 0.357 m_0, respectively. In contrast, under external uniaxial tensile stress, these values are 2.181 and 0.328 m_0, respectively. The corresponding strain tensors with various types of external stress are shown in Table II. The values of the applied stresses are realistic, since besides the original 2.4% biaxial compressive strain induced by lattice mismatch, the reversible change of stress induced by thermal expansion coefficient mismatch (from compressive to tensile state and vice versa), can be achieved in a certain range of temperature [33]. And the uniaxial compressive strain up to 4.8% can be also potentially achieved by selectively etching trenches and regrowing the material layer with larger lattice constant than GaN [34].

Under the external uniaxial stresses, some directions will become dominant when their energies are lowered. The direction with the lowest energy has the highest hole concentration at and around Γ point. Therefore, we expect that the band shape of the 2-D iso-energy contours can determine the mobility behavior. The energy levels of the first subband near Γ point under various types of 8 GPa external stress are presented in Fig. 3. The kinetic energy is used with the inverse sign because the hole states are examined. The subband energy increases with biaxial tensile stress and decreases with biaxial compressive stress. This is consistent with the previous results [35]. In the external uniaxial compression case, the energy of the *A*-*C* direction becomes the lowest, resulting in a hole's repopulation from the *B*-*D* direction to the *A*-*C* direction. On the other hand, in the external uniaxial tension case, the holes are redistributed from the *A*-*C* direction to the *B*-*D* direction, leading to mobility degradation since a much larger effective mass is observed. So we can predict that the hole mobility has the largest increase if the uniaxial compressive stress along the channel is applied. We can also propose another hypothesis that the uniaxial tensile stress perpendicular to the channel is also beneficial for mobility enhancement since in this case the band shape is similar to Fig. 2(c), and the lowest energy also lies on the *A* and *C* directions. The correctness of the assumptions will be discussed by a mobility model in Section III.

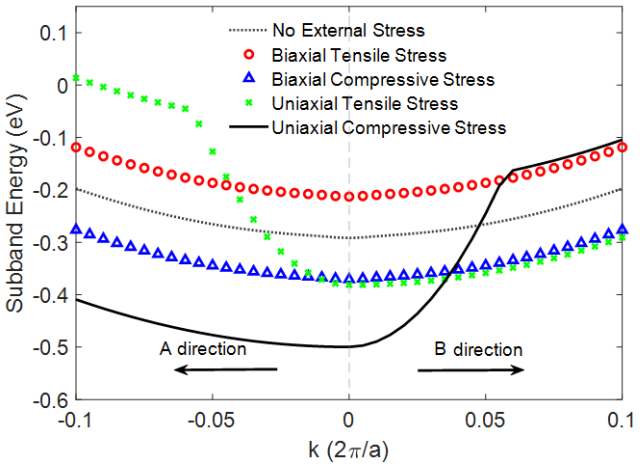

Fig. 3. Comparisons of the first subband energy levels along and perpendicular to current channel under various types of 8 GPa external stress.

III. HOLE MOBILITY ENHANCEMENT MECHANISM UNDER VARIOUS TYPES OF STRESS

According to the discussion in Section II, the uniaxial compressive stress along the channel and the uniaxial tensile stress perpendicular to the channel are predicted to be the better options for hole mobility enhancement. A mobility model based on Kubo–Greenwood formula [30] is used to confirm these hypotheses. The energies of the first pair of subbands are used in the mobility calculation. The higher subbands have little impact on the mobility behavior because carriers stay mostly in the first pair of subbands. The variation of hole mobility with temperature is strongly influenced by acoustic phonon scattering, in addition to the polar optical phonon scattering that dominates in most polar compound semiconductors. Because the holes are highly sensitive to irregularities, such as the correlation length and lateral

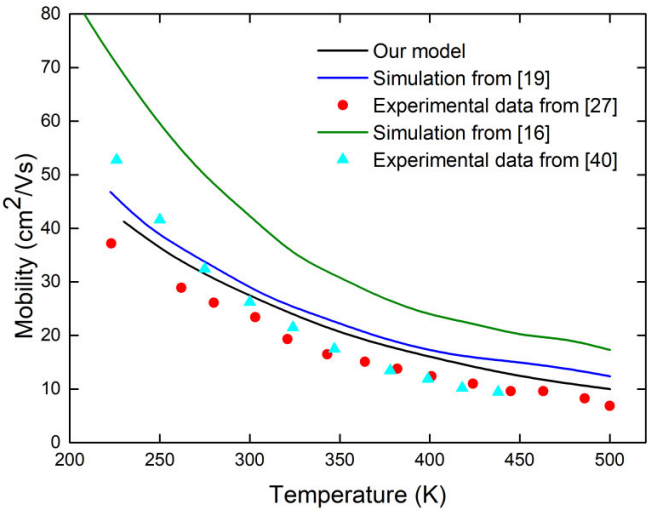

Fig. 4. Calculated hole mobility of GaN/AlN heterojunction QW versus temperature under 2.4% biaxial compressive strain as in [27]. The comparisons with the experimental and theoretical data from [16], [19], [27], and [40] are shown.

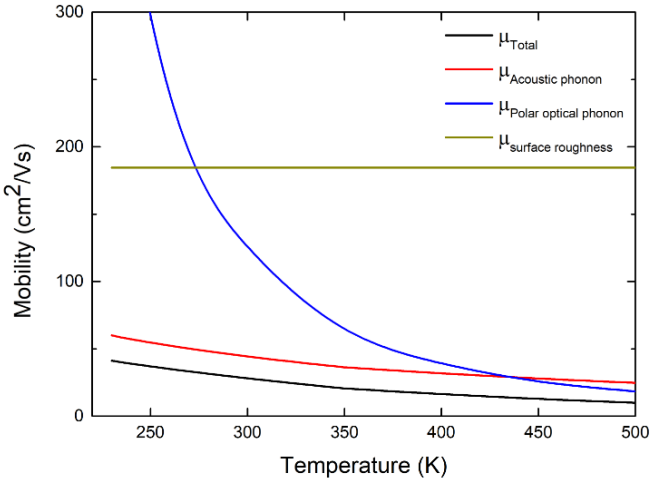

Fig. 5. Temperature dependence of hole mobility of GaN/AlN heterojunction QW due to acoustic phonon scattering, polar optical phonon scattering, and surface roughness scattering, respectively.

size of roughness at the GaN/AlN heterointerface, we also consider the surface roughness scattering which affects the hole transport properties below the room temperature and is seldom ignorable. The anisotropy of the scattering rate due to the subband dispersion can be captured by including their momentum dependence in the model. Other scattering mechanisms, such as dislocation and impurity, are irrelevant to this study, since they either contribute very little at high temperature [36] or can be ignored in the pseudomorphic undoped GaN/AlN heterostructures.

The acoustic phonon and polar optical phonon coupling constants, and the dielectric constants with high and low frequencies extracted from [37], are shown in Table III. For the application of heterojunction in field-effect transistors operating at high power level at and above 300 K, the lateral size of the surface roughness Δ need to be less than 1 nm with a correlation length Λ larger than 5 nm [38]. Since the initial 2.4% biaxial compressive strain has been added in the GaN/AlN heterointerface, we update the scattering

TABLE III
PHONON AND SURFACE ROUGHNESS SCATTERING PARAMETERS

	Symbol	Value	Unit
Acoustic Deformation Potential	Ξ_{eff}	8.3	eV
Optical Phonon energy	$\hbar\omega_{opt}$	91.2	meV
Dielectric Constant (Low Frequency)	ε^0	8.9	F·m^{-1}
Dielectric Constant (High Frequency)	ε^∞	5.35	F·m^{-1}
Correlation length of roughness	Λ	51	Å
Lateral size of roughness	Δ	5.08	Å

TABLE IV
ESTIMATED VALUES OF CORRELATION LENGTH (Λ) AND LATERAL SIZE (Δ) FOR SURFACE ROUGHNESS SCATTERING

Λ (Å)	Δ (Å)
51	5.08
62	7.96
70	8.23
77	8.47
86	8.77
91	8.93
100	9.22
110	9.53
118	9.77
125	9.98

parameters and the temperature dependence of hole mobility in Figs. 4 and 5. Fig. 4 shows the calculated mobility under the corresponding 11.5 GPa initial biaxial compressive stress (2.4% strain). They are still in good agreement with the experimental data. The hole mobility is 27 cm^2/Vs, with the 2DHG density of 5.0×10^{13} cm^{-2} and effective electric field of 0.98 MV/cm at 300 K. Fig. 5 presents the mobility from various scattering mechanism. The tendencies are similar to both the experimental data [22] and theoretical result [19]. The acoustic phonon scattering plays the most important role in the hole mobility around room temperature. The limitation from polar optical phonon scattering becomes more and more significant with the increase of temperature, and turns into the major scattering mechanism above 450 K.

Besides, the mobilities similar to the experimental data can be also obtained by choosing a different set of lateral size and correlation length values [39]. In Table IV, we list the values of Λ and Δ for which the calculated mobility agrees well with the experimental data at $T = 300$ K.

To further illustrate the enhancement mechanism under various types of stress, we show the components of the mobility gain versus external biaxial stress at 300 K in Fig. 6. The 0, 11.5, and 23 GPa points correspond to 2.4% pure biaxial compressive strain, no strain, and 2.4% pure biaxial tensile strain, respectively. The effective mass gain, which is computed assuming the scattering rate is constant, is defined purely as the effect of the band structure (2-D iso-energy contours) change and has been discussed in Section II. The scattering suppression gain, which is associated with the hole

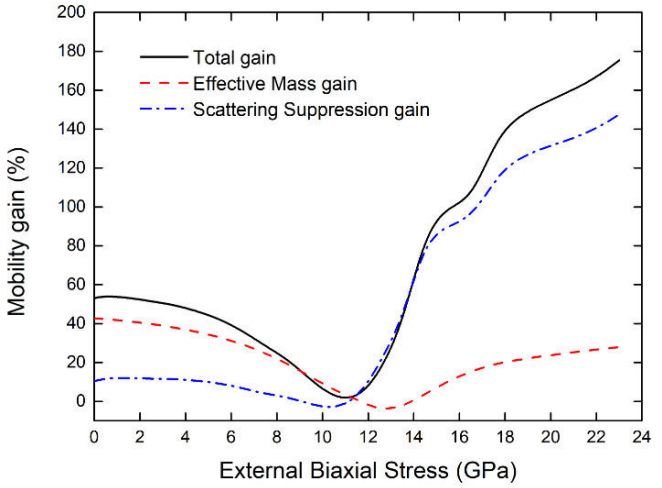

Fig. 6. Mobility gain contribution from effective mass and scattering suppression effect between 2.4% biaxial compressive strain and 2.4% biaxial tensile strain at 300 K. The 0, 11.5, and 23 GPa external biaxial stresses correspond to 2.4% pure biaxial compressive strain, no strain, and 2.4% pure biaxial tensile strain, respectively.

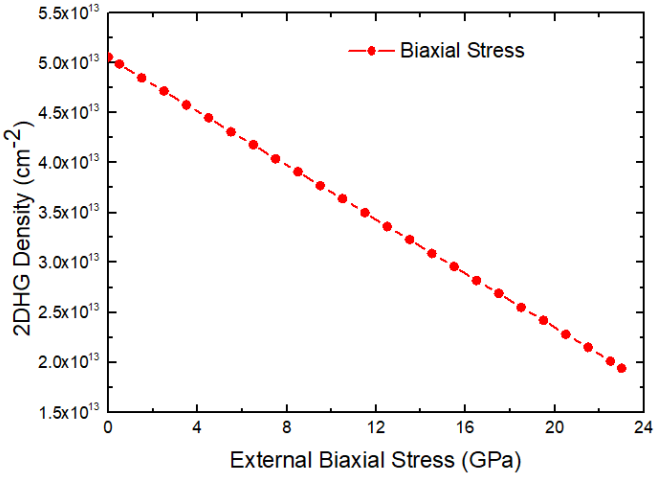

Fig. 7. Relationship between the 2DHG density and external biaxial stress, shows that 3.5 $\times$ 10^{13} cm^{-2} hole density is caused by spontaneous polarization, the rest is caused by piezoelectric polarization.

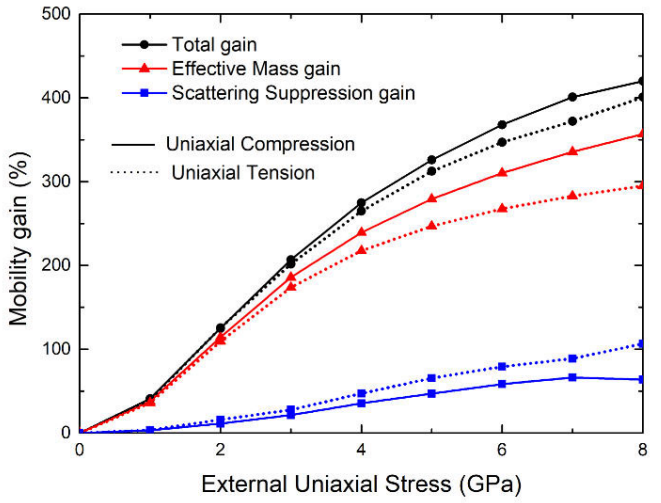

Fig. 8. Mobility gain contribution from effective mass and scattering suppression effects under external uniaxial compressive stress along the channel and uniaxial tensile stress perpendicular to the channel at 300 K.

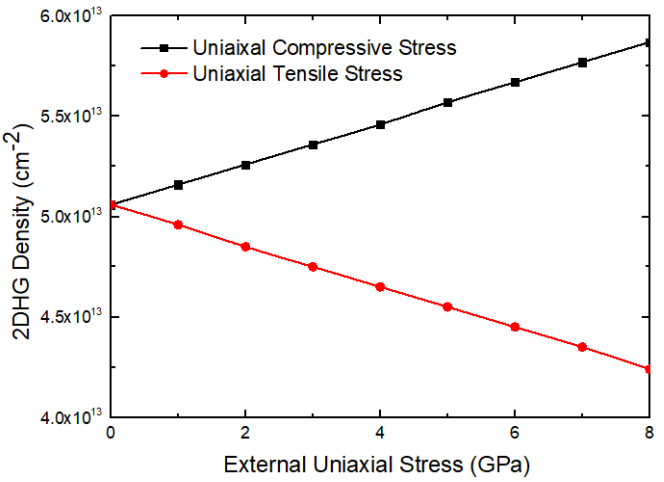

Fig. 9. Changes in the concentration of 2DHG under external uniaxial compressive and tensile stresses.

density, can be computed as the difference between the total gain and effective mass gain. With the reasons of SO and LH bands lifting [16] and the splitting increasing between HH and LH bands [29], the effective mass reduction can be seen under both pure biaxial tensile strain (above 11.5 GPa) and pure biaxial compressive strain (below 11.5 GPa). However, since such effective mass reduction is slight, the feasibility of the mobility enhancement configuration depends on the respective scattering suppression effect. Under the pure 2.4% biaxial compressive strain, even the scattering suppression gain shows a slight gain increase compared to no strain case due to smaller effective mass [38]; this mechanism is still strongly limited because the scattering is enhanced due to the hole redistribution from off-plane to in-plane. The pure biaxial tensile strain has the opposite result, making scattering suppression gain become a dominant component. However, although 2.4% pure biaxial tensile strain can increase the mobility by 180%, a large compressive strain would have to be overcome before this increase can occur. Therefore, it is not a desirable way by applying the external biaxial tensile stress to the GaN/AlN QW in the mobility enhancement. The relationship between the 2DHG and external biaxial stress is presented in Fig. 7. The 2DHG density is roughly equal to the polarization charge. It is also found that about 3.5 $\times$ 10^{13} cm^{-2} hole density is caused by spontaneous polarization.

Fig. 8 presents the gain component at 300 K under the external uniaxial compressive stress along the channel (solid line) and the uniaxial tensile stress perpendicular to the channel (dotted line). The mobility gain is mostly contributed by an effective mass gain in both cases by moving the holes into the low effective mass regions. The scattering suppression gain of the latter one is larger than the former one because of the less hole concentration under tensile stress. Although the in-plane hole concentration increases under compressive stress, the scattering suppression gain still contributes to the mobility gain positively. The reason for that is the energy along the

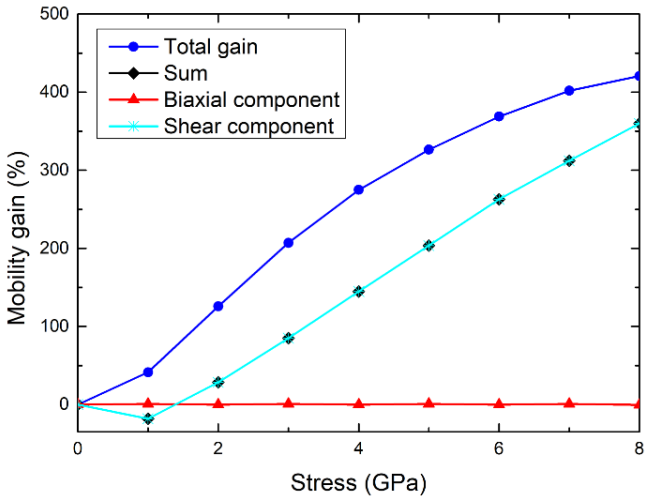

Fig. 10. Contributions from biaxial and shear components of an external uniaxial compressive stress along the current channel at 300 K. The shear component contributes majority of the gain for uniaxial stress and the gains from shear and biaxial add non-linearly.

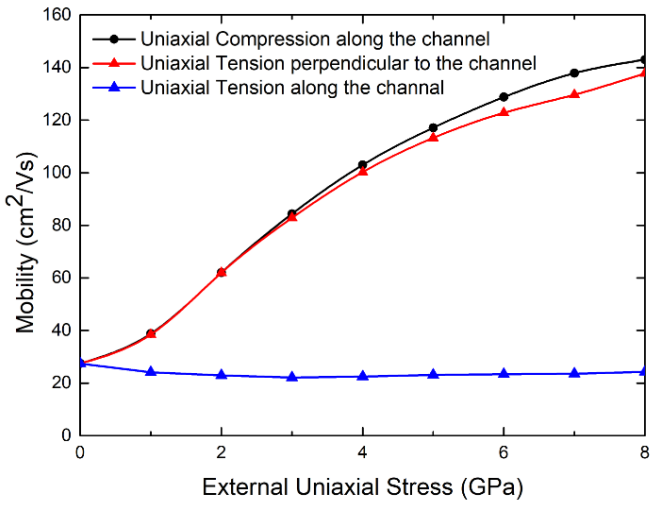

Fig. 11. Hole mobility for various types of uniaxial stress configuration at 300 K. Uniaxial compression stress along the channel direction has the largest mobility gain in all the stress configurations for the same stress level.

A-*C* direction is much lower than others, and the scattering rate for this 135° case is the smallest because of the momentum factor $1 - \cos\theta$ in the scattering rate description [30], in such a way the scattering can be suppressed. The changes in the concentration of 2DHG under external uniaxial compressive and tensile stresses are shown in Fig. 9.

We also plot the mobility gain contribution from shear only and biaxial only and their algebraic sum under external uniaxial compressive stress in Fig. 10. Note that most of the gain is from the shear component, and the dip can be explained by the interrelation between the increasing holes concentration and the scattering suppression effect along *A*-*C* direction. There is almost no influence on mobility gain from the biaxial component alone, revealing that the external biaxial compressive stress is insufficient in the hole mobility enhancement in another way. The interaction of the two components is nonlinear because the total gain from uniaxial compression is larger than the sum of the contributions from each component. So the mobility gain from biaxial compressive stress is much larger when the shear stress is applied than that from biaxial stress alone.

The mobilities versus various types of external in-plane uniaxial stress at 300 K are described in Fig. 11. The uniaxial tensile stress along the channel cannot play an efficient role in the mobility enhancement since the energy of high effective mass regions is moved down. Under the 8 GPa external uniaxial compressive stress along the channel, and the same value of uniaxial tensile stress perpendicular to the channel, the mobility increase from 27 to 143 cm^2/Vs and 137 cm^2/Vs, respectively. In addition, these two enhancement mechanisms are not mutually exclusive; a fin relaxation and a compressive regrowth would complement each other via the Poisson effect to reduce the total amount of stress which each mechanism would have to apply [19]. Such mechanisms combined are shown to increase mobility to 190 cm^2/Vs by further reducing the effective mass and suppressing the scattering.

IV. Conclusion

In this article, we have developed a set of comprehensive physical models to describe the hole mobility enhancement mechanism of (0001)-oriented GaN/AlN heterojunction QW under tensile and compressive stresses. The model is based on the bulk and quantized $k \times p$ method. Anisotropic phonon scattering and surface roughness scattering are included through the Kubo–Greenwood formula. The microscopic relationships among stress, valence QW subband dispersion, and effective mass can be extracted according to the variation of 2-D iso-energy contours. The complex hole mobility behavior under tensile and compressive stresses is explained by the energy movement of the transport plane under stress, the anisotropy scatterings, and the variation of 2DHG density. The satisfactory qualitative (and in several cases also quantitative) agreement is found between experimental data and our theoretical results. The external biaxial tensile stress is shown to move up the in-plane energy, pushing the holes away from the transport plane, and leaving most of its mobility gain from scattering suppression effect. But it is not a desirable way in the mobility enhancement since a large compressive strain induced by the pseudomorphic GaN/AlN heterostructure has to be overcome. The external uniaxial compressive stress along the channel and uniaxial tensile stress perpendicular to channel are considered to be the efficient ways in the hole mobility enhancement. Both configurations are found to move the holes into the direction perpendicular to channel, greatly reducing the effective mass. The ways in achieving scattering suppression are different. The former one pushes the holes into the in-plane regions with the suppressed scattering, while the latter one repopulates the holes from in-plane to off-plane. We hope that this work stimulate experimental research in hole mobility of GaN-based heterojunction, and will accelerate progress toward the wide bandgap p-channel FET and CMOS technology.

References

[1] T. J. Flack, B. N. Pushpakaran, and S. B. Bayne, "GaN technology for power electronic applications: A review," *J. Electron. Mater.*, vol. 45, no. 6, pp. 2673–2682, Mar. 2016, doi: 10.1007/s11664-016-4435-3.

[2] W. Jatal, U. Baumann, K. Tonisch, F. Schwierz, and J. Pezoldt, "High-frequency performance of GaN high-electron mobility transistors on 3C-SiC/Si substrates with Au-free ohmic contacts," *IEEE Electron Device Lett.*, vol. 36, no. 2, pp. 123–125, Feb. 2015, doi: 10.1109/LED.2014.2379664.

[3] M.-H. Mi et al., "90 nm gate length enhancement-mode AlGaN/GaN HEMTs with plasma oxidation technology for high-frequency application," *Appl. Phys. Lett.*, vol. 111, no. 17, Oct. 2017, Art. no. 173502, doi: 10.1063/1.5008731.

[4] B. Romanczyk et al., "Demonstration of constant 8 W/mm power density at 10, 30, and 94 GHz in state-of-the-art millimeter-wave N-polar GaN MISHEMTs," *IEEE Trans. Electron Devices*, vol. 65, no. 1, pp. 45–50, Jan. 2018, doi: 10.1109/TED.2017.2770087.

[5] K. J. Chen et al., "GaN-on-Si power technology: Devices and applications," *IEEE Trans. Electron Devices*, vol. 64, no. 3, pp. 779–795, Mar. 2017, doi: 10.1109/TED.2017.2657579.

[6] Y. Arakawa, K. Ueno, A. Kobayashi, J. Ohta, and H. Fujioka, "High hole mobility p-type GaN with low residual hydrogen concentration prepared by pulsed sputtering," *APL Mater.*, vol. 4, no. 8, Aug. 2016, Art. no. 086103, doi: 10.1063/1.4960485.

[7] T. Fudetani, K. Ueno, A. Kobayashi, and H. Fujioka, "Wide range doping controllability of p-type GaN films prepared via pulsed sputtering," *Appl. Phys. Lett.*, vol. 114, no. 3, Jan. 2019, Art. no. 032102, doi: 10.1063/1.5079673.

[8] B. Reuters et al., "Fabrication of p-channel heterostructure field effect transistors with polarization-induced two-dimensional hole gases at metal–polar GaN/AlInGaN interfaces," *J. Phys. D, Appl. Phys.*, vol. 47, no. 17, Apr. 2014, Art. no. 175103, doi: 10.1088/0022-3727/47/17/175103.

[9] N. Chowdhury et al., "P-channel GaN transistor based on p-GaN/AlGaN/GaN on Si," *IEEE Electron Device Lett.*, vol. 40, no. 7, pp. 1036–1039, Jul. 2019, doi: 10.1109/LED.2019.2916253.

[10] A. Krishna et al., "AlGaN/GaN superlattice-based p-type field-effect transistor with tetramethylammonium hydroxide treatment," *Phys. Status Solidi A*, vol. 217, no. 7, Dec. 2019, Art. no. 1900692, doi: 10.1002/pssa.201900692.

[11] S. J. Bader et al., "Gate-recessed E-mode p-channel HFET with high on-current based on GaN/AlN 2D hole gas," *IEEE Electron Device Lett.*, vol. 39, no. 12, pp. 1848–1851, Dec. 2018, doi: 10.1109/LED.2018.2874190.

[12] R. Chaudhuri, S. J. Bader, Z. Chen, D. Müller, H. G. Xing, and D. Jena, "Molecular beam epitaxy growth of large-area GaN/AlN 2D hole gas heterostructures," *Phys. Status Solidi B*, vol. 257, no. 4, Apr. 2020, Art. no. 1900567, doi: 10.1002/pssb.201900567.

[13] R. Chu, Y. Cao, M. Chen, R. Li, and D. Zehnder, "An experimental demonstration of GaN CMOS technology," *IEEE Electron Device Lett.*, vol. 37, no. 3, pp. 269–271, Mar. 2016, doi: 10.1109/LED.2016.2515103.

[14] A. Nakajima et al., "GaN-based complementary metal–oxide–semiconductor inverter with normally off Pch and Nch MOSFETs fabricated using polarisation-induced holes and electron channels," *IET Power Electron.*, vol. 11, no. 4, pp. 689–694, Feb. 2018, doi: 10.1049/iet-pel.2017.0376.

[15] Z. Zheng et al., "Gallium nitride-based complementary logic integrated circuits," *Nature Electron.*, vol. 4, no. 8, pp. 595–603, Jul. 2021, doi: 10.1038/s41928-021-00611-y.

[16] S. Poncé, D. Jena, and F. Giustino, "Route to high hole mobility in GaN via reversal of crystal-field splitting," *Phys. Rev. Lett.*, vol. 123, no. 9, Aug. 2019, Art. no. 096602, doi: 10.1103/PhysRevLett.123.096602.

[17] S. Poncé, D. Jena, and F. Giustino, "Hole mobility of strained GaN from first principles," *Phys. Rev. B, Condens. Matter*, vol. 100, no. 8, Aug. 2019, Art. no. 085204, doi: 10.1103/PhysRevB.100.085204.

[18] C. Gupta et al., "First demonstration of improvement in hole conductivity in c-plane III-nitrides through application of uniaxial strain," *Jpn. J. Appl. Phys.*, vol. 58, no. 3, Feb. 2019, Art. no. 030908, doi: 10.7567/1347-4065/aaffaa.

[19] S. J. Bader, R. Chaudhuri, M. F. Schubert, H. W. Then, H. G. Xing, and D. Jena, "Wurtzite phonons and the mobility of a GaN/AlN 2D hole gas," *Appl. Phys. Lett.*, vol. 114, no. 25, Jun. 2019, Art. no. 253501, doi: 10.1063/1.5099957.

[20] J. D. Albrecht, P. P. Ruden, and T. L. Reinecke, "Hole scattering near the valence band edge in Wurtzite gallium nitride," *J. Appl. Phys.*, vol. 92, no. 7, pp. 3803–3814, Oct. 2002, doi: 10.1063/1.1503392.

[21] V. A. Jhalani, J.-J. Zhou, and M. Bernardi, "Ultrafast hot carrier dynamics in GaN and its impact on the efficiency droop," *Nano Lett.*, vol. 17, no. 8, pp. 5012–5019, Jul. 2017, doi: 10.1021/acs.nanolett.7b02212.

[22] D. Lancefield and H. Eshghi, "Temperature-dependent hole transport in GaN," *J. Phys., Condens. Matter*, vol. 13, no. 40, pp. 8939–8944, Sep. 2001, doi: 10.1088/0953-8984/13/40/308.

[23] C. Hamaguchi, "Electron and hole mobilities of GaN with bulk, quantum well, and HEMT structures," *J. Appl. Phys.*, vol. 130, no. 12, Sep. 2021, Art. no. 125701, doi: 10.1063/5.0060630.

[24] S.-H. Park and S.-L. Chuang, "Comparison of zinc-blende and Wurtzite GaN semiconductors with spontaneous polarization and piezoelectric field effects," *J. Appl. Phys.*, vol. 87, no. 1, pp. 353–364, Jan. 2000, doi: 10.1063/1.371915.

[25] S. Park, "Crystal orientation effects on electronic properties of Wurtzite GaN-AlGaN quantum Wells_with spontaneous and piezoelectric polarization,," *Jpn. J. Appl. Phys.*, vol. 39, no. 6R, pp. 3478–3482, Jun. 2000, doi: 10.1143/JJAP.39.3478.

[26] F. Mireles and S. E. Ulloa, "Strain and crystallographic orientation effects on the valence subbands of Wurtzite quantum wells," *Phys. Rev. B, Condens. Matter*, vol. 62, no. 4, pp. 2562–2572, Jul. 2000, doi: 10.1103/PhysRevB.62.2562.

[27] R. Chaudhuri, S. J. Bader, Z. Chen, D. A. M´uller, H. G. Xing, and D. Jena, "A polarization-induced 2D hole gas in undoped gallium nitride quantum wells," *Science*, vol. 365, no. 6460, pp. 1454–1457, Sep. 2019, doi: 10.1126/science.aau8623.

[28] Z. Zhang et al., "Polarization-induced 2D hole gases in pseudomorphic undoped GaN/AlN heterostructures on single-crystal AlN substrates," *Appl. Phys. Lett.*, vol. 119, no. 16, Oct. 2021, Art. no. 162104, doi: 10.1063/5.0066072.

[29] Y. Liu, X. Li, G. Zhang, E. X. Wang, and J. Wang, "The calculation for quantized valence subband structure of zinc-blende GaN heterojunction quantum well based on k·p method," *Semicond. Sci. Technol.*, vol. 36, no. 12, Nov. 2021, Art. no. 125011, doi: 10.1088/1361-6641/ac31e0.

[30] Y. Liu, X. Li, E. Wang, G. Zhang, and J. Wang, "Effect of uniaxial compressive stress with different orientations on the hole mobility of Wurtzite GaN heterojunction quantum well," *AIP Adv.*, vol. 12, no. 7, Jul. 2022, Art. no. 075113, doi: 10.1063/5.0089826.

[31] F. Bernardini, V. Fiorentini, and D. Vanderbilt, "Accurate calculation of polarization-related quantities in semiconductors," *Phys. Rev. B, Condens. Matter*, vol. 63, no. 19, Apr. 2001, Art. no. 193201, doi: 10.1103/PhysRevB.63.193201.

[32] Y. Sun, S. E. Thompson, and T. Nishida, "Physics of strain effects in semiconductors and metal-oxide-semiconductor field-effect transistors," *J. Appl. Phys.*, vol. 101, no. 10, May 2007, Art. no. 104503, doi: 10.1063/1.2730561.

[33] J. Keckes et al., "Temperature dependence of stresses in GaN thin films grown on (0001) sapphire: Modeling of thermal stresses," *Appl. Phys. Lett.*, vol. 79, no. 26, pp. 4307–4309, Dec. 2001, doi: 10.1063/1.1427424.

[34] R. Chaudhuri, "Polarization-induced 2D hole gases in undoped (In) GaN/AlN heterostructures," in *Integrated Electronics on Aluminum Nitride*. Cham, Switzerland: Springer, 2022, pp. 62–63.

[35] M. Suzuki and T. Uenoyama, "Strain effect on electronic and optical properties of GaN/AlGaN quantum-well lasers," *J. Appl. Phys.*, vol. 80, no. 12, pp. 6868–6874, Dec. 1996, doi: 10.1063/1.363755.

[36] I. Berdalovic, M. Poljak, and T. Suligoj, "A comprehensive model and numerical analysis of electron mobility in GaN-based high electron mobility transistors," *J. Appl. Phys.*, vol. 129, no. 6, Feb. 2021, Art. no. 064303, doi: 10.1063/5.0037228.

[37] B. E. Foutz, S. K. O'Leary, M. S. Shur, and L. F. Eastman, "Transient electron transport in Wurtzite GaN, InN, and AlN," *J. Appl. Phys.*, vol. 85, no. 11, pp. 7727–7734, Jun. 1999, doi: 10.1063/1.370577.

[38] M. N. Gurusinghe, S. K. Davidsson, and T. G. Andersson, "Two-dimensional electron mobility limitation mechanisms in $Al_xGa_{1-x}N$/GaN heterostructures," *Phys. Rev. B, Condens. Matter*, vol. 72, no. 4, Jul. 2005, Art. no. 045316, doi: 10.1103/PhysRevB.72.045316.

[39] S. Gökden, R. Baran, N. Balkan, and S. Mazzucato, "The effect of interface roughness scattering on low field mobility of 2D electron gas in GaN/AlGaN heterostructure," *Phys. E, Low-Dimensional Syst. Nanostruct.*, vol. 24, nos. 3–4, pp. 249–256, Sep. 2004, doi: 10.1016/j.physe.2004.04.042.

[40] M. Horita et al., "Hall-effect measurements of metalorganic vapor-phase epitaxy-grown p-type homoepitaxial GaN layers with various Mg concentrations," *Jpn. J. Appl. Phys.*, vol. 56, no. 3, Feb. 2017, Art. no. 031001, doi: 10.7567/JJAP.56.031001.